





3 | Editor's Pick | Environmental Microbiology | Research Article

Uncultivated DPANN archaea are ubiquitous inhabitants of global oxygen-deficient zones with diverse metabolic potential

Irene H. Zhang, 1 Benedict Borer, 1 Rui Zhao, 1 Steven Wilbert, 2 Dianne K. Newman, 2,3 Andrew R. Babbin 1

AUTHOR AFFILIATIONS See affiliation list on p. 15.

ABSTRACT Archaea belonging to the DPANN (Diapherotrites, Parvarchaeota, Aenigmarchaeota, Nanoarchaeota, and Nanohaloarchaeota) superphylum have been found in an expanding number of environments and perform a variety of biogeochemical roles, including contributing to carbon, sulfur, and nitrogen cycling. Generally characterized by ultrasmall cell sizes and reduced genomes, DPANN archaea may form mutualistic, commensal, or parasitic interactions with various archaeal and bacterial hosts, influencing the ecology and functioning of microbial communities. While DPANN archaea reportedly comprise a sizeable fraction of the archaeal community within marine oxygen-deficient zone (ODZ) water columns, little is known about their metabolic capabilities in these ecosystems. We report 33 novel metagenome-assembled genomes (MAGs) belonging to the DPANN phyla Nanoarchaeota, Pacearchaeota, Woesearchaeota, Undinarchaeota, lainarchaeota, and SpSt-1190 from pelagic ODZs in the Eastern Tropical North Pacific and the Arabian Sea. We find these archaea to be permanent, stable residents of all three major ODZs only within anoxic depths, comprising up to 1% of the total microbial community and up to 25%-50% of archaea as estimated from read mapping to MAGs. ODZ DPANN appear to be capable of diverse metabolic functions, including fermentation, organic carbon scavenging, and the cycling of sulfur, hydrogen, and methane. Within a majority of ODZ DPANN, we identify a gene homologous to nitrous oxide reductase. Modeling analyses indicate the feasibility of a nitrous oxide reduction metabolism for host-attached symbionts, and the small genome sizes and reduced metabolic capabilities of most DPANN MAGs suggest host-associated lifestyles within ODZs.

IMPORTANCE Archaea from the DPANN (Diapherotrites, Parvarchaeota, Aenigmarchaeota, Nanoarchaeota, and Nanohaloarchaeota) superphylum have diverse metabolic capabilities and participate in multiple biogeochemical cycles. While metagenomics and enrichments have revealed that many DPANN are characterized by ultrasmall genomes, few biosynthetic genes, and episymbiotic lifestyles, much remains unknown about their biology. We report 33 new DPANN metagenome-assembled genomes originating from the three global marine oxygen-deficient zones (ODZs), the first from these regions. We survey DPANN abundance and distribution within the ODZ water column, investigate their biosynthetic capabilities, and report potential roles in the cycling of organic carbon, methane, and nitrogen. We test the hypothesis that nitrous oxide reductases found within several ODZ DPANN genomes may enable ultrasmall episymbionts to serve as nitrous oxide consumers when attached to a host nitrous oxide producer. Our results indicate DPANN archaea as ubiquitous residents within the anoxic core of ODZs with the potential to produce or consume key compounds.

KEYWORDS DPANN, OMZ, archaea, symbiosis, nitrogen cycle enzymes, carbon metabolism, marine microbiology, ODZ

Editor Stephen J. Giovannoni, Oregon State University, Corvallis, Oregon, USA

Address correspondence to Irene H. Zhang, izhang@mit.edu, or Andrew R. Babbin, babbin@mit.edu.

The authors declare no conflict of interest.

See the funding table on p. 16.

Received 26 October 2023 Accepted 22 January 2024 Published 21 February 2024

Copyright © 2024 Zhang et al. This is an open-access article distributed under the terms of the Creative Commons Attribution 4.0 International license.

March 2024 Volume 15 Issue 3

n recent years, metagenomics has enabled the discovery of several prokaryotic superphyla lacking pure culture representatives (1-3). One of these novel groups is the DPANN archaea, named after the first members of the expanding superphylum (Diapherotrites, Parvarchaeota, Aenigmarchaeota, Nanoarchaeota, and Nanohaloarchaeota), which has come to include at least 10 putative phyla (4, 5). The first DPANN described was a Nanoarchaeota, Nanoarchaeum equitans, which remains one of the few cultivated members of the superphylum (6). Since then, DPANN phylogeny has undergone rapid change. Woesearchaeota and Pacearchaeota (formerly Euryarchaea DHVEG-5 and 6, respectively), two of the most ubiquitously distributed DPANN lineages, were reclassified within the superphylum in 2015 (7). Undinarchaeota was recently described as an independent DPANN lineage (5). Apparent unifying features of these DPANN archaea are ultrasmall cell sizes (~0.1–1.5 μm), reduced genomes (~1.5 Mb), and limited metabolic capacities (8). These features, along with several enrichments and visualizations of DPANN archaeal-host associations (6, 9, 10), suggest a symbiotic or commensal lifestyle of DPANN archaea with diverse microbial hosts. Exceptions may exist, including lainarchaeota (formerly Diapherotrites), which has been reported to carry sufficient anabolic capabilities for a free-living lifestyle despite its small genome (11). However, the putative symbiotic lifestyle of the majority of DPANN organisms may explain why they have been challenging to cultivate in isolation.

Since their discovery, DPANN archaea have been found in a variety of diverse environments, including hydrothermal vents (12), freshwater and hypersaline lakes (13, 14), groundwater (15, 16), terrestrial hot springs (17), marine sediments and water columns (12, 18, 19), and the Black Sea (20). Archaea writ large play crucial roles in global biogeochemical cycles, such as in ammonia oxidation (21), methane cycling (22), and organic carbon scavenging (23), and DPANN archaea have been found to possess genes for sulfur cycling and organic substrate degradation (15, 18). Additionally, certain DPANN archaea in anoxic environments may form consortia with methanogens and contribute to anaerobic carbon cycling (24). However, despite their widespread abundance, distribution, and diversity (accounting for about half of all archaeal diversity [8]), the ecological and biogeochemical roles of DPANN archaea are not fully understood. Culture-independent techniques have only begun to unravel the importance of these previously overlooked microorganisms within their expanding list of habitats.

Amplicon surveys have detected the presence of DPANN archaea within both sediments beneath oxygen-deficient zones (ODZs) (25) and the ODZ water column itself (26). The three major oceanic ODZs are located in the eastern tropical North Pacific (ETNP), the eastern tropical South Pacific (ETSP), and the Arabian Sea. Oxygen profiles in these regions display rapid decreases from surface saturation to below the detection limit of trace oxygen sensors (<10 nmol L⁻¹) between 50 and 100 m depth, a region termed the oxycline (27, 28). Oxygen concentrations then remain below detection and with no vertical gradient for approximately 200–800 m (29), although the ODZ thickness varies greatly across each basin (30–32). Due to these unique features, ODZ water columns contain multiple biogeochemical gradients that support diverse microbial assemblages performing nitrogen, carbon, and sulfur cycling (33). In particular, these regions disproportionately contribute to marine nitrogen cycling, accounting for about 30% of marine fixed nitrogen loss despite containing only 0.1–0.2% of oceanic volume (29, 34–36).

ODZs are characterized by prevalent denitrification, i.e., the microbially mediated stepwise reduction of nitrate to dinitrogen gas. This anaerobic respiratory metabolism occurs via reductases encoded by a suite of widely distributed genes (37). The last step of denitrification, the reduction of N_2O to N_2 , is catalyzed by nitrous oxide reductase encoded by *nos*. Two clades of the *nos* catalytic subunit *nosZ* have been found, a typical clade I *nosZ* associated with complete denitrifiers defined by an N-terminal twin-arginine translocation (TAT) motif and an atypical clade II *nosZ* associated with partial denitrifiers defined by an N-terminal Sec-type motif (38). Both variants contain conserved copper-binding sites Cu_A and Cu_Z , although Cu_Z sites of clade II *nosZ* homologs exhibit

greater variability and less conservation (39). Recent studies revealed that clade II nosZ predominates within ODZs, occurs within diverse marine taxa including archaea, and may be associated with low oxygen and enhanced N₂O affinity (39). Because N₂O depletes ozone and is a potent greenhouse gas, organisms with atypical nosZ variants, including archaea, merit interest as potential N₂O sinks.

Increasing attention has been focused on ODZ archaeal communities (40-42), such as members of Thermoproteota (including former Marine Group I Thaumarchaeota) and Thermoplasmatota (including former Marine Group II archaea) (43, 44). However, little is known about ODZ DPANN archaea, despite reports that they may comprise up to 15%-26% of total archaeal reads in coastal ODZs (26). Challenges in the cultivation of these environmental microbes limit our understanding of the metabolic capabilities of clades such as DPANN that lack cultured representatives. We have previously reported a collection of 962 metagenome-assembled genomes (MAGs) from the ETNP and Arabian Sea ODZs (45) and characterized their nitrogen cycling capabilities, focusing on abundant taxa. From this data set, we recovered 33 genomes belonging to DPANN phyla Nanoarchaeota, Pacearchaeota, Woesearchaeota, Undinarchaeota, and Iainarchaeota, several of which carried putative nosZ homologs. However, the contribution of DPANN archaea in ODZ microbial assemblages and biogeochemical cycling, as well as the abundance, distribution, metabolism, ecology, and phylogeny of these archaea remain open questions. We characterize the metabolic capabilities of these ODZ DPANN MAGs, place them within the existing phylogeny of known DPANN, and determine their relative abundances and distributions within and across global ODZs. Our results demonstrate that DPANN are a ubiquitous portion of the microbial community within ODZs and comprise several lineages with diverse metabolic potential.

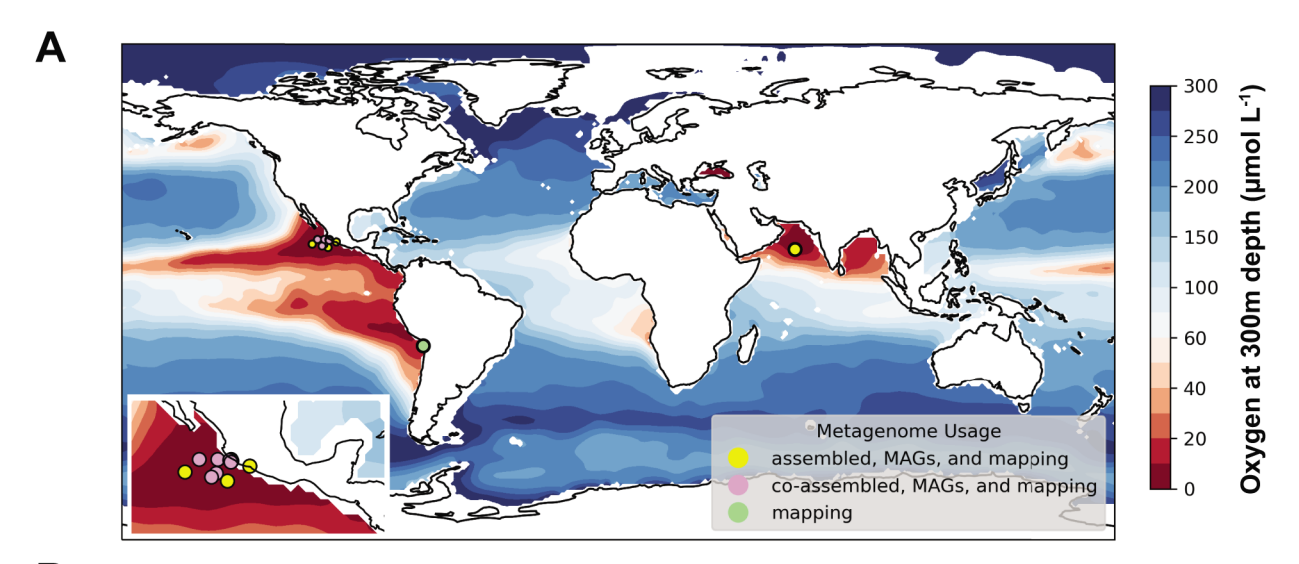
MATERIALS AND METHODS

Sample collection, sequencing, metagenome assembly, and binning

Sampling and sequencing methods for public ETNP metagenomes are described in Fuchsman et al. (42), Glass et al. (46), and Tsementzi et al. (47). Sampling and sequencing methods for public ETSP metagenomes are described in Stewart et al. (48) and Ganesh et al. (49). Raw reads per metagenome were retrieved from the Sequence Read Archive using the following National Center for Biotechnology Information (NCBI) BioProject IDs: PRJNA350692 (Fuchsman ETNP metagenomes), PRJNA254808 (Glass ETNP metagenomes), PRJNA323946 (Tsementzi ETNP metagenomes), PRJNA68419 (Stewart ETSP metagenomes), and PRJNA217777 (Ganesh ETSP metagenomes). Sampling locations for each metagenome were visualized using Python 3.7.12 and the cartopy package. These were plotted against global oxygen concentrations from 300 m below the sea surface from Ocean Data Atlas 2018 (Fig. 1A).

Trimming of raw reads, metagenome assembly, and binning methods are described elsewhere (45). Metagenome-assembled genomes were defined as bins with completion > 50% and contamination < 10% according to CheckM (50), although these statistics based on single-copy genes may underestimate the true completeness of DPANN archaea MAGs due to their limited genome sizes. Taxonomy was assigned to all MAGs using GTDB-tk v1.7.0 with the classify_wf workflow (51). Thirty-three MAGs belonging to DPANN phyla were annotated with PROKKA v1.14.6 (52) against the HAMAP (53) and Pfam databases (54) using the --kingdom Archaea flag. The full set of ODZ MAGs, including all DPANN MAGs analyzed in this study, were deposited under NCBI BioProject ID PRJNA955304. Bioinformatics and modeling code, sequence alignments, and tree files are available at https://github.com/izhang73/DPANN_ODZs. Additionally, MAG names and NCBI BioSample accession numbers for ODZ DPANN archaea are included in a Supplementary Dataset.

Published DPANN MAGs and genomes were manually downloaded from the Joint Genome Institute (JGI), while published DPANN from the National Center for Biotechnology Information were downloaded using the EntrezDirect utility. These DPANN MAGs



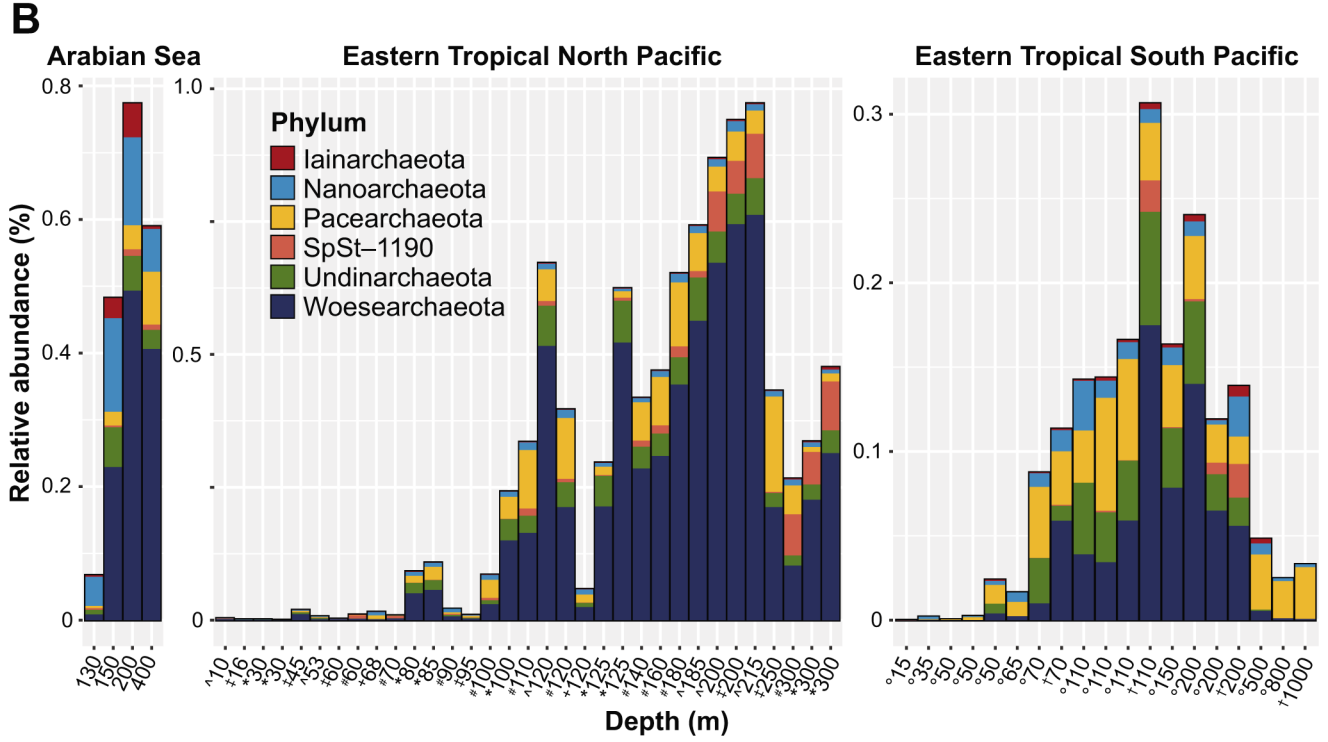


FIG 1 Metagenome-assembled genomes of DPANN archaea from oxygen-deficient zones. (A) Locations of metagenomes from ETNP, ETSP, and Arabian Sea used for metagenome assembly, MAG binning, and relative abundance mapping. (B) Relative abundances of DPANN MAGs across metagenome samples, color-coded by phylum-level taxonomy. Depths are listed for each of the samples. Arabian Sea: all samples are from 2007 (45); ETNP: ^ indicates samples from 2016 (45), ‡ indicates samples from 2018 (45), * indicates samples from 2013 (46), # indicates samples from 2012 (42), + indicates samples from 2013 (47); and ETSP: † indicates samples from 2008 (48), and ° indicates samples from 2010 (49). Map is adapted from Zhang et al. (45).

and genomes were assessed for completeness and contamination with CheckM v1.0.12 (50), and detailed taxonomy was determined with GTDB-tk v1.7.0 (51). MAGs and genomes below 50% completion and above 10% contamination, along with those that did not taxonomically classify within DPANN phyla, were pruned, and the remaining genomes were dereplicated with dRep v3.2.2 (55) with the -sa 0.99 flag to remove redundant genomes.

TARA Oceans MAGs were retrieved from Delmont et al. (56). To determine if DPANN MAGs were present within the TARA Oceans collection, we reclassified the 957

non-redundant TARA Oceans MAGs with GTDB-tk v1.7.0 (51). These taxonomies were then searched for the presence of any DPANN phyla.

For dereplicated ODZ DPANN MAGs, coverage mapping was performed with CoverM using the flags minimap2-sr --min-read-aligned-percent 50 --min-read-percent-identity 0.95 --min-covered-fraction 0 (https://github.com/wwood/CoverM). Relative abundances of dereplicated MAGs resulting from CoverM mapping were visualized using R v4.1.3 and the packages phyloseq, ggplot2, and dplyr.

Gene searching, metabolic analysis, and tree building

Unique published DPANN and all ODZ DPANN MAGs were queried for 76 archaea-specific single copy genes, which were aligned using GToTree v1.6.31 with the -H Archaea -G 0.25 flags (57). We created a phylogenetic tree based on the output archaeal single copy gene alignment with IQ-Tree v1.6.12 (58) using the WAG + R6 model and 1,000 ultrafast bootstraps (59).

To determine the metabolic capabilities of ODZ DPANN, we used Anvi'o v7.1 (60). Briefly, for each DPANN MAG, we generated a contigs database with anvi-gen-contigs-database. For metabolic predictions, we ran anvi-run-kegg-kofams to search against the KOfam HMM database of Kyoto Encyclopedia of Genes and Genomes (KEGG) orthologs (61) and automatically assigned hits above the KEGG bitscore thresholds for each KOfam profile. Additionally, we ran anvi-run-ncbi-cogs to search against the NCBI Clusters of Orthologous Groups (COGs) database (62) and identified archaeal single-copy core genes using anvi-run-hmms -I Archaea 76. To predict the presence or absence of metabolic pathways, we ran anvi-estimate-metabolism on each MAG. We annotated a metabolic pathway as present if over 70% of the genes in the pathway are present in a MAG, and partially present if 33%–70% of the genes in a pathway are present in a MAG. Additionally, we searched for annotations of genes of interest within PROKKA annotations for each MAG, particularly for genes involved in fermentation, aerobic or anaerobic respiration, and energy metabolism. Sequences belonging to genes of interest were retrieved from each MAG and further inspected.

Protein sequences belonging to positive hits for denitrification genes from ODZ DPANN MAGs were obtained for nosZ. We extracted and aligned with MAFFT v7.450 using the --auto and --leavegappyregion parameters. Alignments were visualized in JalView v2.11.2.6 (63) and inspected for alignment quality and the conservation of key enzymatic regions for nosZ. Prediction of membrane-bound regions, protein localization, and protein structure were determined via DeepTMHMM (64). To create a protein tree for nosZ, bacterial and archaeal nosZ-encoded protein sequences were obtained from NCBI using the query esearch -db protein -query "NosZ" | efetch -format fasta, and sequences under 200 amino acids and over 800 amino acids were removed. In addition, cytochrome c oxidase subunit II proteins from bacteria and archaea were downloaded from NCBI using the queries esearch -db protein -query "cytochrome c oxidase subunit ii [PROT] AND bacteria [ORGN]" | efetch -format fasta and esearch -db protein -query "cytochrome c oxidase subunit ii [PROT] AND archaea [ORGN]" | efetch -format fasta. Sequences under 200 amino acids and over 800 amino acids were removed. To remove redundant or very similar sequences, Usearch v11 was used to cluster NCBI nosZ and cytochrome c oxidase subunit II (Cox2) sequences at 90% amino acid identity with the flags -cluster_fast -id 0.9 -centroids (65). From clustered Cox2 sequences, 15 Cox2 sequences from taxonomically diverse organisms were chosen at random. These selected Cox2 were concatenated with clustered nosZ sequences and DPANN nosZ sequences and aligned with MAFFT v7.450 (66) using the --auto and --leavegappyregion flags. The resulting Cox2 and nosZ alignment was trimmed with trimAl 1.4.1 with the -automated1 flag (67). We used the trimmed alignment to create a maximum likelihood protein tree using IQ-Tree v1.6.12 with 1,000 ultrafast bootstraps.

10.1128/mbio.02918-23 6

Research Article mBio

Methods for modeling producer and consumer dynamics

We used COMSOL (v5.6) to simulate the concentration field and associated uptake rate around a two-cell system consisting of a producer and consumer in three-dimensional space. In this simulation, the producer cell is represented as a sphere with a constant relative concentration of 1 on its surface. The consumer cell on the other hand is represented by a sphere with a relative concentration of 0 on its surface. We represent all aqueous concentrations as relative concentrations between producer and consumer cells since the estimation of an absolute cell surface concentration for the producer requires precise (as yet unknown) knowledge of an individual cell's N2O production or consumption rate. We then strategically vary the relative radius of the producer (R) and consumer (r) cells, and the distance between the surface of the two cells (d) to disentangle the influence of these different factors on the relative substrate uptake of the consumer cell. A list of parameters and their values can be found in Table S2, which we cross-combine to create a total of 100 simulations. The whole simulation domain is a square domain of 20 µm side length with the consumer and producer cells equidistant from the center in the horizontal plane. The relative concentration field around the producer and consumer cells is predicted by solving the diffusion equation (equation 1) at steady state, where J is the flux of N_2O (m⁻² s⁻¹), D is the diffusion coefficient (m² s⁻¹), and $\frac{\partial C}{\partial x} + \frac{\partial C}{\partial y} + \frac{\partial C}{\partial z}$ the spatial N₂O gradients (m⁻⁴). We impose a relative concentration of 0 at the boundary of the domain and surface of the consumer cell (reflecting the background nitrous oxide concentration) and 1 at the cell surface of the producer. Cellular uptake of the consumer cell is calculated by the three-dimensional integration of this equation across the cell surface.

$$J = D\left(\frac{\partial C}{\partial x} + \frac{\partial C}{\partial y} + \frac{\partial C}{\partial z}\right) \tag{1}$$

Genetic engineering methods and determining N2O concentrations

We inserted DNA sequences derived from DPANN putative nitrous oxide reductase genes into a *Pseudomonas aeruginosa* strain PA14 model system on a plasmid integrated into the genomic attTn7 site (68). Production and consumption of N₂O by these cultures were quantified using a microelectrode (Unisense, Denmark). Details are provided in the Supplemental Methods.

RESULTS

DPANN within the ODZ archaeal community

From a set of 962 MAGs > 50% completion and <10% contamination binned from the ETNP and Arabian Sea ODZs (45), 33 MAGs were taxonomically assigned to the DPANN superphylum, with 23 Woesearchaeota, 2 Pacearchaeota, 2 Nanoarchaeota, 1 lainarchaeota, 3 Undinarchaeota, and 2 MAGs assigned to SpSt-1190, also known as Candidatus Altiarchaeota. The novel SpSt-1190 phylum was previously characterized in hydrothermal vents (12) but not in marine water columns. While our Woesearchaeota and Pacearchaeota MAGs were classified by GTDB-tk as members of Nanoarchaeota, phylogenetic analyses confirmed their placement within these phyla (Fig. 2). DPANN MAGs mapped to ODZ metagenomes within all three ODZs, including ETSP and ETNP metagenomes spanning multiple cruises, sampling sites, and years (Fig. 1A). However, no DPANN MAGs were recovered from oxygenated surface metagenomes from the ETNP. Searching the TARA Oceans data set comprising 957 non-redundant MAGs from co-assemblies from the global surface oceans (<10 m depth) and deep chlorophyll maxima (10-100 m depth) revealed no MAGs belonging to ODZ DPANN groups, and only two DPANN MAGs, both of which originated from the Red Sea and were assigned to Halobacteriota. The remainder of the 87 archaeal MAGs from TARA Oceans were assigned

March 2024 Volume 15 Issue 3

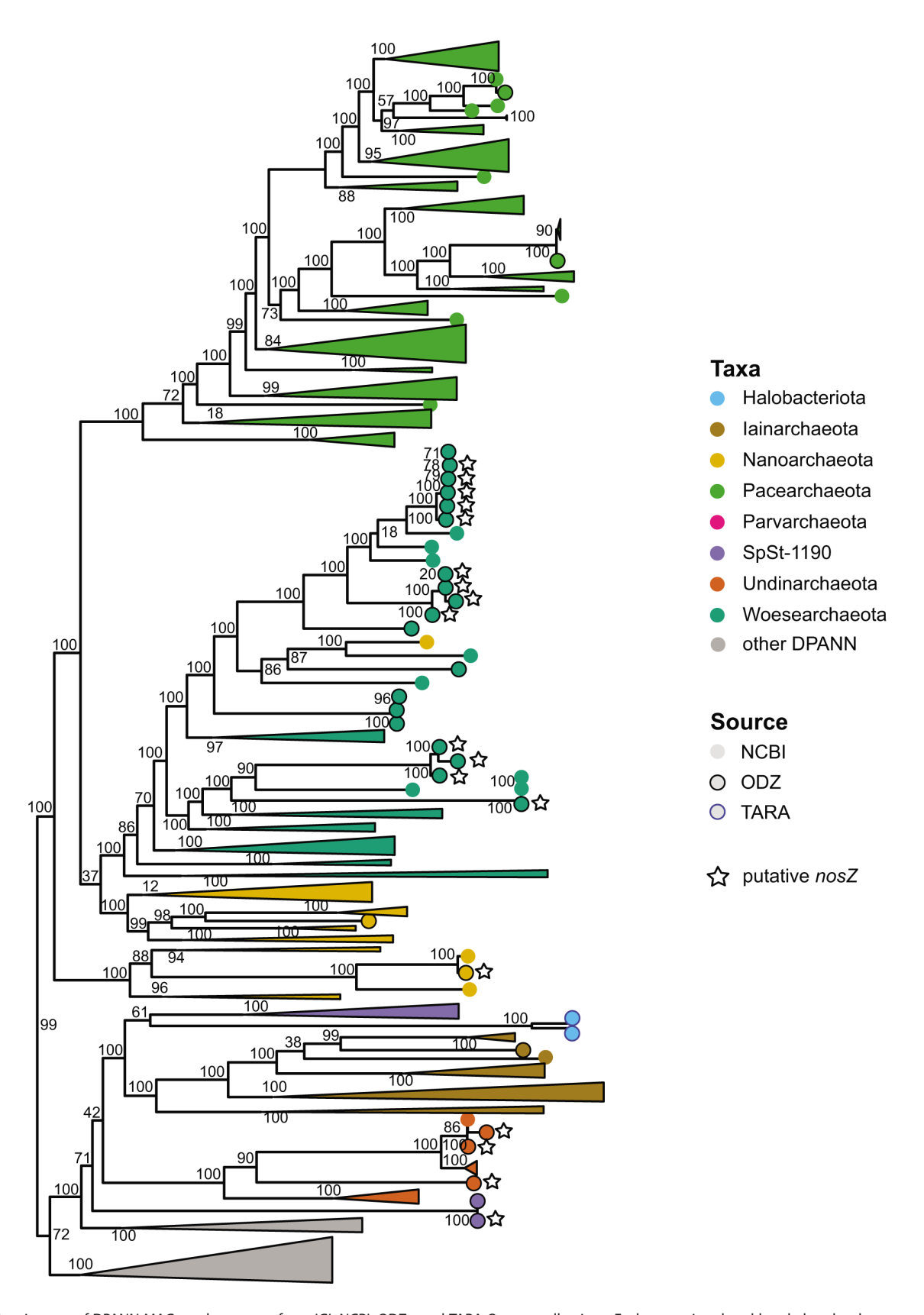


FIG 2 Species tree of DPANN MAGs and genomes from JGI, NCBI, ODZs, and TARA Oceans collections. Each group is colored by phylum-level taxonomy. Only DPANN phyla containing ODZ or TARA MAGs are shown. Black outlined circles indicate ODZ MAGs, blue outlined circles indicate TARA Oceans MAGs, and circles without outlines indicate NCBI or JGI genomes. Stars next to tips indicate the presence of a putative *nosZ*-like gene. Numbers by nodes correspond to bootstrap supports.

to either Thermoplasmatota or Thermoproteota. From 962 ODZ MAGs, 169 archaeal MAGs include 133 Thermoplasmatota or Thermoproteota, 2 Hydrothermarchaeota, and 1 Methanobacteriota to complement the 33 DPANN archaea. The average completion of retrieved ODZ DPANN MAGs was 75% with an average contamination of 2.6%. Dereplication at 99% average nucleotide identity resulted in 16 unique MAGs (one lainarchaeota, two Nanoarchaeota, one SpSt-1190, three Undinarchaeota, one Pacearchaeota, and eight Woesearchaeota).

The archaeal population within ODZs, as represented by mapping to non-redundant archaeal ODZ MAGs, peaked within the oxycline above the ODZ core, with archaeal MAGs comprising 14% of the microbial community at 80 m depth in the ETNP (Fig. S1A). At these depths, Thermoplasmatota and Thermoproteota dominated, with DPANN MAGs present at 0.25% relative abundance or less. DPANN MAGs also mapped to a few reads from surface metagenomes from either the ETNP or ETSP, indicating low or absent populations of ODZ DPANN groups in surface waters (Fig. 1B). No surface waters from the Arabian Sea were sampled. Within the anoxic ODZ core, DPANN archaea comprised about 25%-50% of the archaeal community (Fig. S1B). The highest relative abundances occurred around 200 m depth in the ETNP (about 1% of the total community and 50% of the archaeal community) and the Arabian Sea (about 0.8% of the total community and 27% of the archaeal community) (Fig. 1B; Fig. S1B). In the ETSP, relative abundances were lower (about 0.3% of the total community and 25% of the archaeal community) but peaked approximately at the same depths (100-200 m). While abundances and distributions were similar across the various ODZs, the Arabian Sea harbored a comparatively larger proportion of Nanoarchaeota, although Woesearchaeota were still the most abundant fraction in general. The ETSP and ETNP were primarily dominated by Woesearchaeota with smaller contributions by Pacearchaeota, SpSt-1190, and Undinarchaeota (Fig. 1B).

A phylogenetic tree of ODZ DPANN MAGs along with MAGs and genomes retrieved from NCBI and JGI revealed that ODZ Woesearchaeota MAGs fall within one primary clade, although several Woesearchaeota MAGs branched within other groups (Fig. 2). Sister taxa falling next to ODZ Woesearchaeota were derived from Mariana Trench surficial sediments, coral reefs, and groundwater metagenomes from NCBI. However, ODZ MAGs belonging to the Pacearchaeota and Nanoarchaeota did not cluster together within these phyla, indicating that these MAGs are not closely related to each other despite their common environment. The two SpSt-1190 MAGs from ODZs branched outside of the SpSt-1190 clade and potentially form a distinct lineage from other SpSt-1190.

Carbon metabolism within ODZ DPANN archaea

Metabolic analysis of ODZ DPANN MAGs showed diverse metabolic capabilities across MAGs but limited metabolic and biosynthetic pathways within each MAG (Fig. 3). Metabolic capabilities described are based upon annotations against the KEGG and COGs databases and require functional verification. While these annotations are predictions only, they offer estimates of metabolic potential for these uncultured organisms. Regarding anabolic synthesis, MAGs belonging to Nanoarchaeota had the most limited capabilities, with the absence of glycolysis of three-carbon compounds, no tricarboxylic acid (TCA) cycle genes, no pentose phosphate pathways, no pathways detected for the biosynthesis of most amino acids, and limited biosynthetic pathways for purine nucleotides. The absence of these pathways, even when considering these as partial genomes, suggests extremely limited abilities to synthesize purines, amino acids, lipids, vitamins, and other necessary cellular components. Other DPANN MAGs possessed more metabolic capabilities, although most lacked evidence of complete glycolysis, TCA cycle, and pathways for the synthesis of multiple essential amino acids. Our draft Woesearchaeota genomes possessed partial or complete capabilities for the last stages of glycolysis, the non-oxidative or reductive portions of the pentose phosphate pathway, and pyruvate oxidation. Additionally, most were capable of partial or complete purine

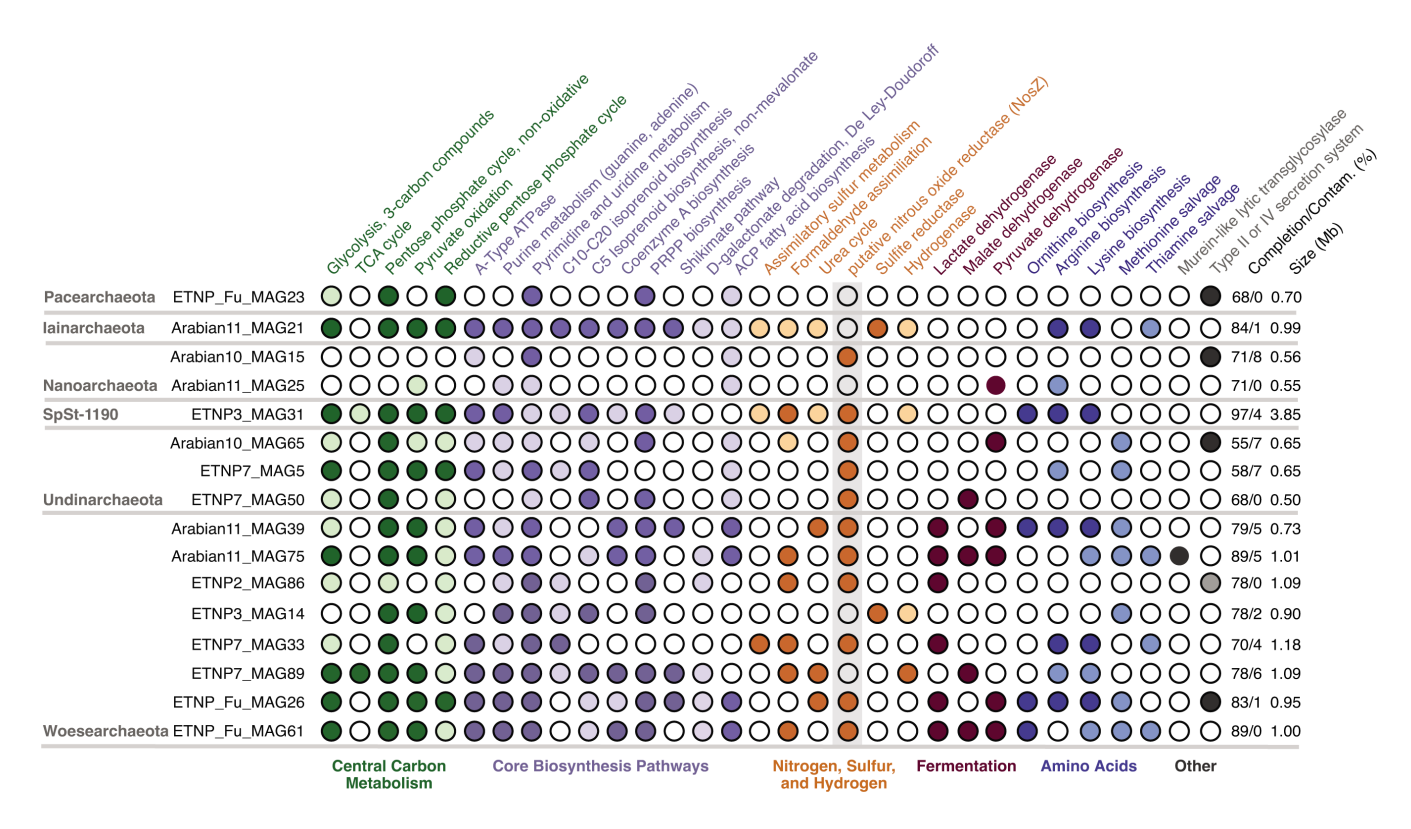


FIG 3 Metabolic analysis of unique DPANN MAGs. Circles show the presence/absence of key metabolic pathways, grouped by color according to general metabolism categories. Darker circles indicate >70% of genes within the pathway are present, while lighter circles indicate partial pathways (33%–70% present). White circles indicate <33% of genes are present, and the pathway is considered absent. Completion/contamination and size of MAGs are shown on the right.

and pyrimidine biosynthesis. Other central carbon archaeal pathways varied, with most MAGs lacking the shikimate pathway for the biosynthesis of aromatic amino acids (69), the biosynthesis pathway for the ubiquitous cofactor coenzyme A, and the DeLey-Doudoroff pathway for galactose utilization, which is analogous to the Entner-Doudoroff pathway (70). Several MAGs lacked the ability to synthesize the intermediate phosphoribosyl diphosphate used in building nucleotides, some amino acids, and essential cofactors (71), as well as biosynthesis pathways for isoprenoids (Fig. 3).

In accordance with other published DPANN archaea (4, 6, 9), the genome sizes of most ODZ DPANN were small, averaging 1.05 Mb. The exceptions were MAGs belonging to SpSt-1190, which had genome sizes of 4 Mb. DPANN MAGs encoded for a number of transporters, including ones for zinc, iron, magnesium, and other metals, biotin transporters, SemiSWEET transporters for cellular uptake and translocation of sugars, and other ABC-type transporters. Peptidases, particularly signal peptidases and membrane-bound peptidases, were also widespread. Seven DPANN MAGs from four phyla contained genes for Type II or IV secretion systems associated with protein transport and DNA exchange across membranes. Additionally, three DPANN MAGs encoded a murein-like lytic transglycosylase (1, 7). Normally absent in archaea, these large proteins bind and degrade peptidoglycan strands such as in bacterial cell walls (72).

Several DPANN MAGs possessed the 3-oxoacyl-ACP reductase FabG, enoyl-ACP reductase FabI, and 3-hydroxyacyl-ACP dehydratase FabZ. These acyl carrier protein (ACP) fatty acid biosynthesis genes are typically found within bacteria and eukaryotes, which possess a bacterial pathway for lipid biosynthesis, the methylerythritol phosphate (MEP) pathway, while typical archaea use the non-homologous mevalonate (MVA) pathway. This "lipid divide" is a central distinguishing feature between archaea and bacteria (3). We found a distinction between Woesearchaeota and Nanoarchaeota MAGs, which possessed the MEP pathway, while SpSt-1190, Undinarchaeota, Pacearchaeota,

and lainarchaeota contained genes for the MVA pathway. Further BLAST searching of DPANN ACP pathway proteins against the NCBI non-redundant protein database revealed high sequence similarity to other protein sequences from DPANN archaea, although the next highest scoring hits primarily belonged to bacteria. Additionally, five Woesearchaeota DPANN MAGs carried genes for cyclopropane fatty acid phospholipid synthesis, which are used in stabilizing bacterial phospholipid membranes (73) but have not been previously reported in archaea.

Energy metabolism and nutrient cycling within ODZ DPANN archaea

Lactate, malate, and pyruvate dehydrogenases were present in seven out of eight unique Woesearchaeota and two out of three unique Undinarchaeota MAGs, indicating fermentative capabilities (Fig. 3). These genes were absent in most Pacearchaeota, Nanoarchaeota, SpSt-1190, and lainarchaeota MAGs. Two unique DPANN MAGs (Arabian11_MAG21 and ETNP3_MAG14) also carried the A and B subunits of assimilatory anaerobic sulfite reductase, but none carried dissimilatory sulfur cycling genes. Additionally, several DPANN MAGs contained desulfoferredoxin, manganese superoxide dismutases, and thioredoxin, which are involved in antioxidant systems (16), despite living in anoxic water columns. Formaldehyde assimilation genes were found within a number of Woesearchaeota MAGs, suggesting the ability to use one-carbon compounds for growth. MAGs belonging only to SpSt-1190 also encoded nearly complete pathways for methanogenesis, along with a number of other methane metabolisms including the ribulose monophosphate pathway and methanofuran biosynthesis.

Several DPANN MAGs encoded hydrogenases (Fig. 3), with two MAGs (ETNP3_MAG31 and ETNP7_MAG89) encoding an FeFe-type hydrogenase potentially used in fermentative metabolism, while two (Arabian11_MAG21 and ETNP3_MAG14) encoded an NiFe-type hydrogenase that may catalyze hydrogen oxidation for energy, which has recently been shown to be widespread among archaea (73) and marine bacteria (74). Additionally, several ODZ DPANN (Arabian11_MAG21, ETNP3_MAG31, Arabian11_MAG39, ETNP7_MAG89, and ETNP_Fu_MAG26) contained genes for urea cycling. These metabolic capabilities indicate diverse roles in carbon, sulfur, hydrogen, and nitrogen cycling for DPANN archaea within ODZs.

Potential nitrous oxide reduction capability within ODZ DPANN

Within our 33 DPANN MAGs, 21 encoded a gene annotated as the *nosZ* gene for nitrous oxide reductase, which catalyzes the reduction of N₂O to N₂. An HMM search against the HMM profile from validated *nosZ* sequences returned expectation values between 8.4 × 10^{-17} and 2.2×10^{-5} and bit scores from 57.9 to 20.1, compared to canonical *nosZ e*-values of less than 1.2×10^{-33} and bit scores > 113. In comparison, cytochrome c oxidase subunit II proteins returned expectation values of $0.003-7.5 \times 10^{-5}$ and bit scores of 13–18.4. While bit score cutoffs vary, a bit score > 50 is considered almost always significant (75).

However, other denitrification genes were absent within these MAGs. A gene tree built with canonical *nosZ* from bacteria and archaea, the DPANN *nosZ*-like protein, and the closely related homolog cytochrome c oxidase subunit II protein indicated that DPANN *nosZ*-like genes comprised a monophyletic clade branching in between Cox2 and clade II Sec-type *nosZ* (Fig. 4). Further investigation of multiple-sequence protein alignments of *nosZ*-encoded nitrous oxide reductase and the DPANN *nosZ*-like protein revealed the presence of a conserved copper-binding site, the Cu_A site, which has been reported within *nosZ* and Cox2 proteins. This site is exemplified by the C₁X₃C₂X₃H binding motif (76–78). The Cu_Z catalytic site typically found within *nosZ* was not found within the DPANN *nosZ*-like proteins, and DPANN *nosZ*-like proteins were shorter (56–617 amino acids) than canonical *nosZ* proteins (200–796 amino acids, although sequences varied in completeness). The Cu_Z site, which lacks a specific conserved motif, is characterized by seven conserved histidine residues (38, 78, 79). Within two DPANN MAGs (ETNP8_MAG25 and ETNP3_MAG31), we found a short cupredoxin-like domain protein directly upstream of the *nosZ*-like protein containing five conserved histidine

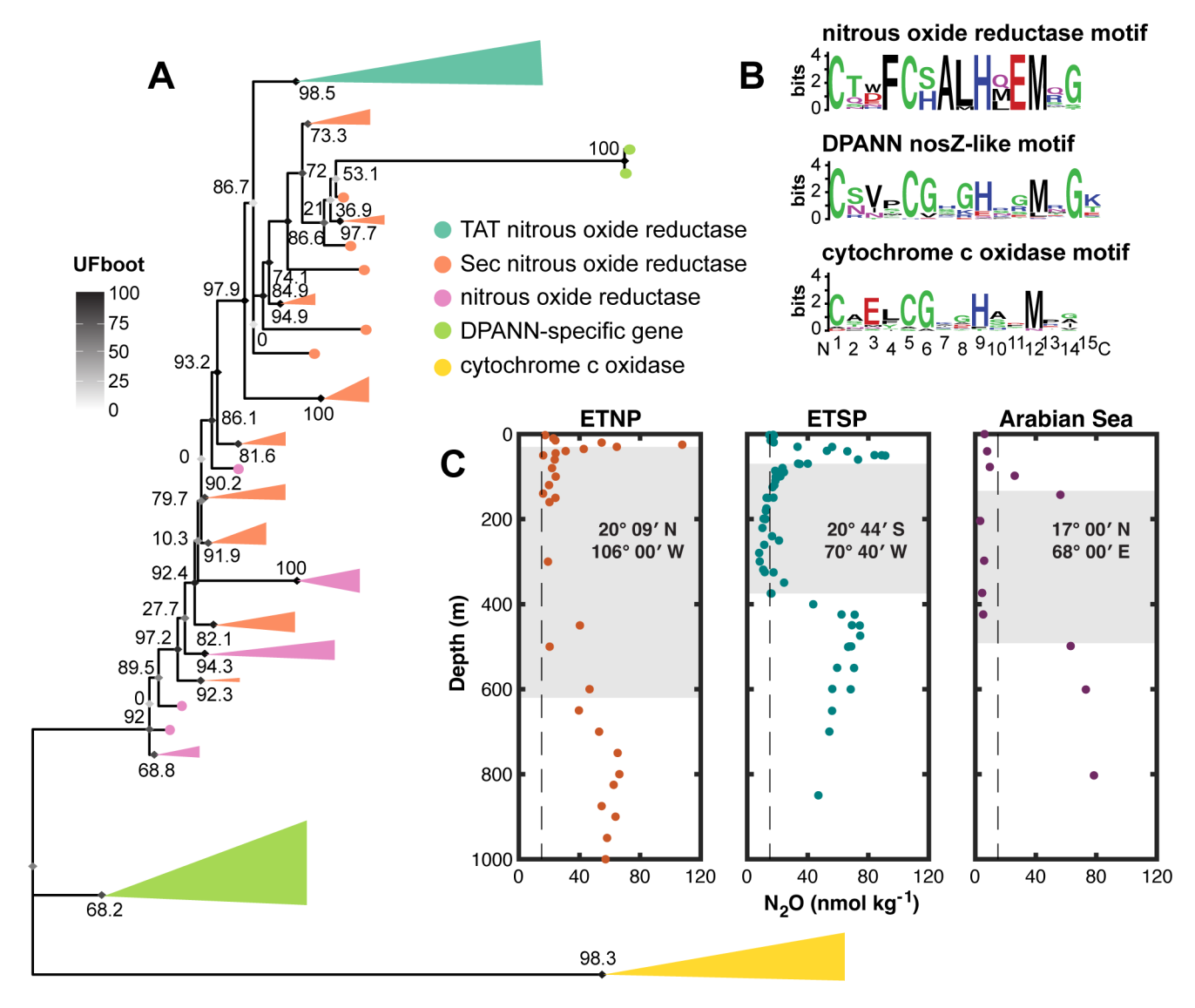


FIG 4 Protein tree of DPANN *nosZ*-like proteins (green) within the larger tree of canonical *nosZ* proteins (typical TAT type in teal, atypical Sec type in orange, and type unknown in pink). Tree is rooted on cytochrome c oxidase subunit II proteins, shown in yellow. Diamonds at nodes correspond to ultrafast bootstrap (UFboot) supports, while numbers are SH-aLRT values. (B) Sequence motifs for the conserved Cu_A copper-binding site for each protein. (C) Historical nitrous oxide concentration profiles are replotted from the oxygen-deficient zones of the Eastern Tropical North Pacific (80), Eastern Tropical South Pacific (81, 82), and the Arabian Sea (83).

residues, which clustered with clade II nosZ sequences containing the Cu_Z site within the protein phylogeny (Fig. 4).

The mature NosZ protein resides in the periplasmic space in known denitrifiers (38). Predictions of protein location for NCBI nosZ sequences and the DPANN nosZ-like gene indicated that both contain a signal sequence followed by the majority of the protein located outside the inner membrane, perhaps indicating a function more similar to nosZ (Fig. S2). In contrast, the Cox2 protein contained two transmembrane regions. A heterologous complementation test performed by separately introducing three DPANN nosZ-like sequences into a Pseudomonas aeruginosa $\Delta nosZ$ mutant did not yield significant differences in N2O consumption between P. aeruginosa $\Delta nosZ$ with DPANN nosZ-like gene insertion vs the $\Delta nosZ$ parent strain (Fig. S3). One strain carrying a putative DPANN nosZ-like gene variant displayed reduced N2O concentrations compared to the $\Delta nosZ$ parent, indicating potential N2O consumption, but this difference was not statistically significant (P = 0.26). Our positive control, the wild-type P. aeruginosa PA14

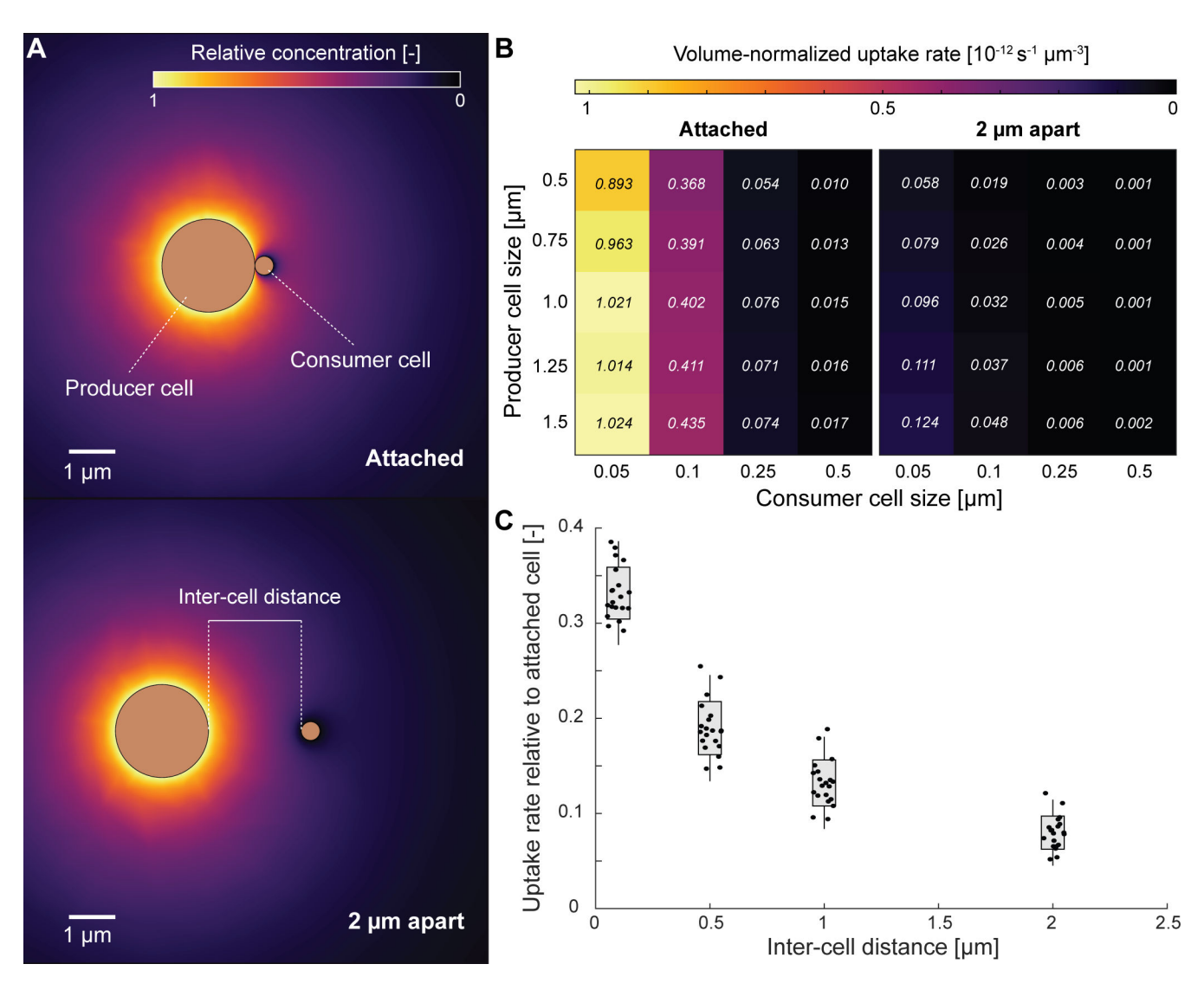


FIG 5 (A) Schematic showing the spatial N_2O concentration for two inter-cell distances of d=0 µm (attached) and d=2 µm (free living). The relative surface N_2O concentration for the producer is set to 1, while the relative surface N_2O concentration of the consumer is set to 0. The radius of the producer, the radius of the consumer, and the distance between the cells are varied according to the values in Table S2. (B) Volume-normalized uptake rate of N_2O for the consumer at 0 µm separation (attached) and 2 µm separation (free living) for all values of the consumer and producer cell sizes. Numbers indicate the actual volume-normalized uptake rates (multiplied by 10^{-12}). (C) Uptake rates as a function of the inter-cell distance normalized to the attached scenario of the same consumer-producer cell size combination. A value of, e.g., 0.2 indicates that this combination of producer and consumer cell size shows a reduction of 80% in the consumer N_2O uptake rate at this distance compared to if they were attached. The spread within a given inter-cell distance is a result of varying the producer and consumer cell sizes (cross-combining five consumer with four producer sizes as shown in panel B). n=20 simulations plotted for each bar, with box representing ± 1 s.d. and the whiskers showing ± 2 s.d.

containing a functional *nosZ* gene, displayed reduced N_2O concentrations (P < 0.001), validating the ability of our experimental system to detect N_2O reduction ability.

 N_2O in the ODZ typically exists at bulk nanomolar concentrations (84), raising the question of whether specialization on N_2O consumption is metabolically feasible. However, local N_2O concentrations may vary in the presence of N_2O producers such as partial denitrifiers carrying upstream denitrification capabilities. We simulated the conditions under which local N_2O concentrations differ from bulk conditions by varying a set of parameters representing the distance between the N_2O consumer and N_2O producer and the size ratio of the two cells (Fig. 5). Generally, two conditions favored elevated N_2O uptake rates for the consumer normalized to cell volume: when the

consumer cell was small relative to the producer cell (Fig. 5B) and when the distance between the producer and consumer cells was small (Fig. 5C). Rates were normalized to cell volume to reflect the important consideration that resource requirements are proportional to cell size (85). Consumer cell size has a decisive influence on the N2O uptake rate for two reasons. First, a smaller cell size directly increases the uptake rate normalized to cell volume, allowing a cell to obtain relatively more resources. Second, a large producer-to-consumer size ratio surrounds the consumer cell within the diffusive boundary layer of the producer cell, increasing the absolute concentrations a consumer sees and thus again increasing the volume-normalized uptake rate. For example, an increase in the ratio of consumer-to-producer radii from ~0.1 to ~1 resulted in an average 100-fold decrease in N₂O uptake for attached consumer cells. Similarly, increasing the producer cell size threefold increased the attached consumer N₂O uptake rate from ~14% for small consumer cells to 67% for larger consumer cells. Incredibly, increasing distances between cells from 0 to 0.1 μm reduced the maximal N₂O uptake rate by ~65% on average, and a consumer cell merely 2 µm from a producer received 93% less than those attached (Fig. 5C). Therefore, when bulk N₂O was low, as in the ODZ (80), consumer cells experienced high N₂O supply only when they were in physical contact with an N₂O producer ($d = 0 \mu m$) and when they were much smaller in size relative to the producer, as would be the case for episymbiotic DPANN archaea.

DISCUSSION

DPANN archaea were found to be a stable resident population within all three permanent pelagic ODZs. Abundances of DPANN archaea, including Nanoarchaeota, SpSt-1190, lainarchaeota, Woesearchaeota, and Undinarchaeota, increase as oxygen decreases, while few or no DPANN archaea were found in the surface oceans (Fig. 1B). While a few population differences were found between ODZs, Woesearchaeota were the dominant phylum within all three ODZs, with Nanoarchaeota in the Arabian Sea and Pacearchaeota, Undinarchaeota, and SpSt-1190 in the ETNP and ETSP forming the next most abundant groups (Fig. 1B).

ODZ DPANN archaea were phylogenetically and metabolically diverse and grouped together with other DPANN from non-ODZ environments, although several Woesearchaeota clustered within the same clade (Fig. 2). Similar to DPANN across various environments (4, 12, 14, 15), most ODZ DPANN had small genome sizes and limited capacity for the biosynthesis of essential amino acids and nucleotides, limited energetic capabilities, and partial or absent pentose phosphate pathways despite overall high MAG completion estimates (Fig. 3). Additionally, completion metrics may underestimate the completeness of DPANN MAGs due to their limited genomes and high number of absent genes considered essential in other organisms. Numerous studies have reported microscopy images of environmental DPANN attached to host cells (6, 15, 86). While most ODZ DPANN genomes suggest a host-associated rather than free-living lifestyle, SpSt-1190 genomes averaged 4 Mb in size, possessed a number of biosynthesis pathways, and carried pathways for methanogenesis. ODZs contain large reservoirs of oceanic methane, the bulk of which has been ascribed to sedimentary methanogenesis (87). SpSt-1190 may represent novel free-living DPANN organisms (88-90) involved in water column methane cycling.

Studies have suggested the role of DPANN archaea in carbon cycling, such as by scavenging organic carbon in the form of nucleotides, lipids, and amino acids (23, 91), participating in the exchange of carbon compounds with hosts, and even directly parasitizing upon hosts (14). In addition, some may perform fermentation and consume or produce acetate (8). We found conserved pathways for amino acid salvage and fermentation across ODZ DPANN genomes (Fig. 3). While various sugar, protein, and DNA transporters indicated potential resource exchange with host cells, the existence of a peptidoglycan-degrading enzyme and secreted peptidases within several MAGs may point to a potentially parasitic relationship between the host and DPANN cell. Future experimental tests will be needed to clarify these metagenomic predictions. The

identification of ODZ DPANN hosts, whether a single host, various hosts, or a community, may hold keys to their distribution and survival within ODZ environments.

While other nitrogen cycling genes were absent, a majority of ODZ DPANN carried a gene similar to the nitrous oxide reductase gene nosZ that catalyzes the reduction of nitrous oxide (N2O) to N2. Further investigation of this gene, annotated as nitrous oxide reductase, indicated the presence of a conserved Cu_A copper-binding site typical of nosZ and cytochrome c oxidase subunit II (77, 78) (Fig. 4). The cellular location of the protein product of the DPANN nosZ-like gene was postulated as outside of the membrane, possibly in the periplasmic space (Fig. S2). DPANN archaea are thought to possess two membranes (92), and canonical nosZ is a periplasmic protein unlike the membrane-bound cytochrome c oxidase subunit II (76). Cytochrome c oxidase performs the last step of aerobic respiration, but no other components of aerobic respiration, such as other cytochrome oxidase subunits or electron transport chain proteins, were found within these archaea (Fig. 3). The Cuz catalytic center, typically found upstream of the Cu_A center in nosZ, was absent within DPANN nosZ-like genes. The Cu_Z center lacks a consensus motif but is characterized by seven histidine residues that bind copper ions (93). While the majority of DPANN MAGs possessed several acyl carrier protein genes for fatty acid biosynthesis surrounding the nosZ-like gene, two DPANN MAGs encoded a protein containing five histidine residues directly upstream of the nosZ-like gene. This protein, annotated to the same family as nosZ, grouped phylogenetically with clade II nosZ sequences (Fig. 4) and may perform a function related to that of the Cu_Z site. This hypothetical histidine-rich region was absent within other DPANN MAGs and was not included in the complementation test. The activity of these or other proteins within these genomes may be required for N2O reduction. While the function of putative nosZ-like genes within DPANN archaea remains hypothetical, their presence only in ODZs and conservation within these small, streamlined genomes suggest the involvement of these genes in N₂O reduction or another redox process with metabolic or physiological importance for ODZ DPANN.

Complementation of *P. aeruginosa* $\Delta nosZ$ with DPANN nosZ-like genes did not result in significant N₂O consumption. While heterologous complementation may offer convincing evidence for the function of unknown genes, negative results are difficult to interpret. Large evolutionary distances between DPANN archaea and the Gram-negative bacterium *P. aeruginosa*, likely resulting in different intracellular conditions, may inhibit the proper transcription, translation, or maturation of the DPANN NosZ-like protein. The protein may also be adapted to specific environmental conditions necessary for its activity, which differ from those used during standard cultivation of *P. aeruginosa*. Deletion and complementation of the nosZ-like gene within native DPANN archaea would be an ideal functional test, but currently, no cultured representatives or genetic toolkits are available for these organisms, limiting our knowledge of many of their metabolic features to predictions from gene annotations.

 N_2O exists in nanomolar concentrations in ODZs compared to the higher concentrations of nitrate and nitrite (84), posing challenges for N_2O -reducing specialists lacking upstream denitrification genes. However, an N_2O -consuming lifestyle may be feasible if local N_2O concentrations are elevated in proximity to an N_2O source, such as a partial denitrifier lacking *nosZ*. Previous studies have indicated the widespread occurrence of partial denitrifiers lacking *nosZ* within ODZ regions (42, 45). We tested this scenario by modeling the local flux of N_2O from a producer (the source) to an N_2O consumer (Fig. 5). The N_2O uptake rate of the consumer was elevated 100-fold when the two cells are in physical contact vs when they are a short distance of 2 μ m away (Fig. 5C). However, this increase in N_2O uptake rate dropped off steeply as the consumer-to-producer cell size ratio increased (Fig. 5). Under low bulk N_2O concentrations, partial denitrifiers may provide elevated local N_2O only to much smaller surface-attached episymbiotic N_2O consumers. DPANN archaea within ODZs, similar to those found within other environments (6, 9, 15), potentially exist as host-associated episymbionts and likely possess small cell sizes. The average cell volume of DPANN archaea has been reported as 0.004

 μm^3 (15), while the average marine bacterial cell volume has been reported at up to 0.096 μm^3 (94), resulting in a consumer-to-producer cell size ratio of <0.05. Thus, DPANN archaea may be uniquely adapted to consume N₂O and other resources that are scarce under bulk conditions but locally elevated in proximity to host cells.

DPANN archaea possess a high number of unknown or unannotated genes, representing "microbial dark matter." Within our ODZ DPANN, we found over 20,000 hypothetical proteins across all MAGs. Further studies, possibly using genetic manipulations, isolation or enrichment cultures, imaging, and computational proteomics approaches are required to characterize the functions of putative or hypothetical proteins. The expanding knowledge of these organisms may make these questions more tractable in the near future. At a large scale, the scavenging of carbon, potential nitrogen, sulfur, and hydrogen cycling capabilities, and ecological effects on host populations via symbiosis or parasitism by DPANN archaea in the ODZs warrant future investigation.

ACKNOWLEDGMENTS

We thank Dr. Xin Sun (Carnegie Institution for Science) and Dr. Bess B. Ward, Dr. Amal Jayakumar, and Dr. Samantha G. Fortin (Princeton University) for sample collection, DNA extractions, and providing the resulting metagenomics data we used to assemble MAGs for this study. We are also grateful for the generosity of Dr. Bruce Heflinger in supporting the Bablab, including this work.

Funding for this project came from the Simons Foundation award 622065 and the National Science Foundation award OCE-2142998 to A.R.B. I.H.Z. was supported in part by an MIT School of Science MathWorks Science Fellowship, and B.B. was supported in part by a Swiss National Science Foundation fellowship (P500PN_202842). Grants to S.W. (from the National Science Foundation Graduate Fellowship Program) and to D.K.N. (from the NIH, R01 HL152190-03) also contributed.

I.H.Z. and A.R.B. conceptualized this study. I.H.Z. assembled metagenomes and MAGs, conducted bioinformatics analyses, and drafted the paper. B.B. and A.R.B. conceived and carried out analyses regarding the N₂O uptake model. R.Z. provided bioinformatics and overall guidance. D.K.N. and S.W. conceived the heterologous complementation test for the *nosZ* homologs and provided all strains used in this study, and S.W. performed genetic engineering within the *Pseudomonas* model system.

AUTHOR AFFILIATIONS

¹Department of Earth, Atmospheric and Planetary Sciences, Massachusetts Institute of Technology, Cambridge, Massachusetts, USA

²Division of Biology and Biological Engineering, California Institute of Technology, Pasadena, California, USA

³Division of Geological and Planetary Sciences, California Institute of Technology, Pasadena, California, USA

PRESENT ADDRESS

Irene H. Zhang, Department of Biological Sciences–Marine and Environmental Biology, University of Southern California, Los Angeles, California, USA

AUTHOR ORCIDs

Irene H. Zhang http://orcid.org/0000-0002-9118-6933

Benedict Borer http://orcid.org/0000-0002-1801-1088

Rui Zhao http://orcid.org/0000-0002-6013-9587

Dianne K. Newman http://orcid.org/0000-0003-1647-1918

Andrew R. Babbin http://orcid.org/0000-0002-5046-0609

FUNDING

Funder	Grant(s)	Author(s)
National Science Foundation (NSF)	OCE-2142998	Andrew R. Babbin
Simons Foundation (SF)	622065	Andrew R. Babbin
HHS National Institutes of Health (NIH)	R01 HL152190-03	Dianne K. Newman

AUTHOR CONTRIBUTIONS

Irene H. Zhang, Conceptualization, Data curation, Formal analysis, Investigation, Methodology, Writing – original draft, Writing – review and editing | Benedict Borer, Conceptualization, Formal analysis, Investigation, Methodology, Visualization, Writing – original draft, Writing – review and editing | Rui Zhao, Conceptualization, Formal analysis, Methodology, Validation, Writing – review and editing | Steven Wilbert, Investigation, Methodology, Resources, Validation, Writing – review and editing | Dianne K. Newman, Funding acquisition, Methodology, Resources, Supervision, Writing – review and editing | Andrew R. Babbin, Conceptualization, Funding acquisition, Investigation, Methodology, Project administration, Resources, Supervision, Writing – review and editing

ADDITIONAL FILES

The following material is available online.

Supplemental Material

Supplemental Material (mBio02918-23-S0001.pdf). Supplemental text, Tables S1 and S2, and Figures S1-S3.

Information on MAGs and accession numbers (mBio02918-23-S0002.xlsx). Names, NCBI accession numbers, completeness, contamination, size, and other information for each MAG.

REFERENCES

- Rinke C, Schwientek P, Sczyrba A, Ivanova NN, Anderson IJ, Cheng J-F, Darling A, Malfatti S, Swan BK, Gies EA, Dodsworth JA, Hedlund BP, Tsiamis G, Sievert SM, Liu W-T, Eisen JA, Hallam SJ, Kyrpides NC, Stepanauskas R, Rubin EM, Hugenholtz P, Woyke T. 2013. Insights into the phylogeny and coding potential of microbial dark matter. Nature 499:431–437. https://doi.org/10.1038/nature12352
- Hug LA, Baker BJ, Anantharaman K, Brown CT, Probst AJ, Castelle CJ, Butterfield CN, Hernsdorf AW, Amano Y, Ise K, Suzuki Y, Dudek N, Relman DA, Finstad KM, Amundson R, Thomas BC, Banfield JF. 2016. A new view of the tree of life. Nat Microbiol 1:16048. https://doi.org/10. 1038/nmicrobiol.2016.48
- Castelle CJ, Banfield JF. 2018. Major new microbial groups expand diversity and alter our understanding of the tree of life. Cell 172:1181– 1197. https://doi.org/10.1016/j.cell.2018.02.016
- Dombrowski N, Lee J-H, Williams TA, Offre P, Spang A. 2019. Genomic diversity, lifestyles and evolutionary origins of DPANN archaea. FEMS Microbiol Lett 366:fnz008. https://doi.org/10.1093/femsle/fnz008
- Dombrowski N, Williams TA, Sun J, Woodcroft BJ, Lee J-H, Minh BQ, Rinke C, Spang A. 2020. Undinarchaeota illuminate DPANN phylogeny and the impact of gene transfer on archaeal evolution. Nat Commun 11:3939. https://doi.org/10.1038/s41467-020-17408-w
- Huber H, Hohn MJ, Rachel R, Fuchs T, Wimmer VC, Stetter KO. 2002. A new phylum of archaea represented by a nanosized hyperthermophilic symbiont. Nature 417:63–67. https://doi.org/10.1038/417063a
- Castelle CJ, Wrighton KC, Thomas BC, Hug LA, Brown CT, Wilkins MJ, Frischkorn KR, Tringe SG, Singh A, Markillie LM, Taylor RC, Williams KH, Banfield JF. 2015. Genomic expansion of domain archaea highlights roles for organisms from new phyla in anaerobic carbon cycling. Curr Biol 25:690–701. https://doi.org/10.1016/j.cub.2015.01.014
- Castelle CJ, Brown CT, Anantharaman K, Probst AJ, Huang RH, Banfield JF. 2018. Biosynthetic capacity, metabolic variety and unusual biology in

- the CPR and DPANN radiations. Nat Rev Microbiol 16:629–645. https://doi.org/10.1038/s41579-018-0076-2
- Baker BJ, Comolli LR, Dick GJ, Hauser LJ, Hyatt D, Dill BD, Land ML, Verberkmoes NC, Hettich RL, Banfield JF. 2010. Enigmatic, ultrasmall, uncultivated archaea. Proc Natl Acad Sci USA 107:8806–8811. https://doi.org/10.1073/pnas.0914470107
- Comolli LR, Banfield JF. 2014. Inter-species interconnections in acid mine drainage microbial communities. Front Microbiol 5:367. https://doi.org/ 10.3389/fmicb.2014.00367
- Youssef NH, Rinke C, Stepanauskas R, Farag I, Woyke T, Elshahed MS. 2015. Insights into the metabolism, lifestyle and putative evolutionary history of the novel archaeal phylum 'Diapherotrites'. ISME J 9:447–460. https://doi.org/10.1038/ismej.2014.141
- Cai R, Zhang J, Liu R, Sun C, Atomi H. 2021. Metagenomic insights into the metabolic and ecological functions of abundant deep-sea hydrothermal vent DPANN archaea. Appl Environ Microbiol 87:e03009-20. https://doi.org/10.1128/AEM.03009-20
- Cabello Yeves PJ, Zemskaya TI, Zakharenko AS, Sakirko MV, Ivanov VG, Ghai R, Rodriguez - Valera F. 2020. Microbiome of the deep Lake Baikal, a unique oxic bathypelagic habitat. Limnology & Oceanography 65:1471–1488. https://doi.org/10.1002/lno.11401
- Vigneron A, Cruaud P, Lovejoy C, Vincent WF. 2022. Genomic evidence of functional diversity in DPANN archaea, from oxic species to anoxic vampiristic consortia. ISME Commun 2:4. https://doi.org/10.1038/ s43705-022-00088-6
- He C, Keren R, Whittaker ML, Farag IF, Doudna JA, Cate JHD, Banfield JF. 2021. Genome-resolved metagenomics reveals site-specific diversity of episymbiotic CPR bacteria and DPANN archaea in groundwater ecosystems. Nat Microbiol 6:354–365. https://doi.org/10.1038/s41564-020-00840-5

- Gios E, Mosley OE, Weaver L, Close M, Daughney C, Handley KM. 2023. Ultra-small bacteria and archaea exhibit genetic flexibility towards groundwater oxygen content, and adaptations for attached or planktonic lifestyles. ISME Commun 3:13. https://doi.org/10.1038/ s43705-023-00223-x
- Chen L-X, Méndez-García C, Dombrowski N, Servín-Garcidueñas LE, Eloe-Fadrosh EA, Fang B-Z, Luo Z-H, Tan S, Zhi X-Y, Hua Z-S, Martinez-Romero E, Woyke T, Huang L-N, Sánchez J, Peláez AI, Ferrer M, Baker BJ, Shu W-S. 2018. Metabolic versatility of small archaea Micrarchaeota and Parvarchaeota. ISME J 12:756–775. https://doi.org/10.1038/s41396-017-0002-z
- Lannes R, Cavaud L, Lopez P, Bapteste E. 2021. Marine ultrasmall prokaryotes likely affect the cycling of carbon, methane, nitrogen, and sulfur. Genome Biol Evol 13:evaa261. https://doi.org/10.1093/gbe/ evaa261
- Liu X, Wang Y, Gu J-D. 2021. Ecological distribution and potential roles of Woesearchaeota in anaerobic biogeochemical cycling unveiled by genomic analysis. Comput Struct Biotechnol J 19:794–800. https://doi. org/10.1016/j.csbj.2021.01.013
- Suominen S, Dombrowski N, Sinninghe Damsté JS, Villanueva L. 2021. A
 diverse uncultivated microbial community is responsible for organic
 matter degradation in the Black Sea sulphidic zone. Environ Microbiol
 23:2709–2728. https://doi.org/10.1111/1462-2920.14902
- Könneke M, Bernhard AE, de la Torre JR, Walker CB, Waterbury JB, Stahl DA. 2005. Isolation of an autotrophic ammonia-oxidizing marine archaeon. Nature 437:543–546. https://doi.org/10.1038/nature03911
- Boetius A, Ravenschlag K, Schubert CJ, Rickert D, Widdel F, Gieseke A, Amann R, Jørgensen BB, Witte U, Pfannkuche O. 2000. A marine microbial consortium apparently mediating anaerobic oxidation of methane. Nature 407:623–626. https://doi.org/10.1038/35036572
- Li M, Baker BJ, Anantharaman K, Jain S, Breier JA, Dick GJ. 2015. Genomic and transcriptomic evidence for scavenging of diverse organic compounds by widespread deep-sea archaea. Nat Commun 6:8933. https://doi.org/10.1038/ncomms9933
- Liu X, Li M, Castelle CJ, Probst AJ, Zhou Z, Pan J, Liu Y, Banfield JF, Gu J-D. 2018. Insights into the ecology, evolution, and metabolism of the widespread Woesearchaeotal lineages. Microbiome 6:102. https://doi. org/10.1186/s40168-018-0488-2
- Besseling MA, Hopmans EC, Boschman RC, Sinninghe Damsté JS, Villanueva L. 2018. Benthic archaea as potential sources of tetraether membrane lipids in sediments across an oxygen minimum zone. Biogeosciences 15:4047–4064. https://doi.org/10.5194/bg-15-4047-2018
- Sollai M, Villanueva L, Hopmans EC, Keil RG, Sinninghe Damsté JS. 2019. Archaeal sources of intact membrane lipid biomarkers in the oxygen deficient zone of the Eastern tropical South Pacific. Front Microbiol 10:765. https://doi.org/10.3389/fmicb.2019.00765
- Tiano L, Garcia-Robledo E, Dalsgaard T, Devol AH, Ward BB, Ulloa O, Canfield DE, Peter Revsbech N. 2014. Oxygen distribution and aerobic respiration in the north and south Eastern tropical Pacific oxygen minimum zones. Deep Sea Research Part I: Oceanographic Research Papers 94:173–183. https://doi.org/10.1016/j.dsr.2014.10.001
- Revsbech NP, Larsen LH, Gundersen J, Dalsgaard T, Ulloa O, Thamdrup B.
 2009. Determination of ultra-low oxygen concentrations in oxygen minimum zones by the STOX sensor. Limnology & Ocean Methods 7:371–381. https://doi.org/10.4319/lom.2009.7.371
- Kwiecinski JV, Babbin AR. 2021. A high-resolution tlas of the Eastern tropical Pacific oxygen deficient zones. Global Biogeochemical Cycles 35:e2021GB007001. https://doi.org/10.1029/2021GB007001
- Ward BB, Devol AH, Rich JJ, Chang BX, Bulow SE, Naik H, Pratihary A, Jayakumar A. 2009. Denitrification as the dominant nitrogen loss process in the Arabian sea. Nature 461:78–81. https://doi.org/10.1038/ nature08276
- 31. Babbin AR, Keil RG, Devol AH, Ward BB. 2014. Organic matter stoichiometry, flux, and oxygen control nitrogen loss in the ocean. Science 344:406–408. https://doi.org/10.1126/science.1248364
- Babbin AR, Buchwald C, Morel FMM, Wankel SD, Ward BB. 2020. Nitrite oxidation exceeds reduction and fixed nitrogen loss in anoxic Pacific waters. Marine Chemistry 224:103814. https://doi.org/10.1016/j. marchem.2020.103814

 Ulloa O, Canfield DE, DeLong EF, Letelier RM, Stewart FJ. 2012. Microbial oceanography of anoxic oxygen minimum zones. Proc Natl Acad Sci USA 109:15996–16003. https://doi.org/10.1073/pnas.1205009109

- 34. Codispoti LA, Brandes JA, Christensen JP, Devol AH, Naqvi SWA, Paerl HW, Yoshinari T. 2001. The oceanic fixed nitrogen and nitrous oxide budgets: moving targets as we enter the anthropocene?. Sci. Mar 65:85–105. https://doi.org/10.3989/scimar.2001.65s285
- DeVries T, Deutsch C, Rafter PA, Primeau F. 2013. Marine denitrification rates determined from a global 3-D inverse model. Biogeosciences 10:2481–2496. https://doi.org/10.5194/bg-10-2481-2013
- Bianchi D, Dunne JP, Sarmiento JL, Galbraith ED. 2012. Data-based estimates of suboxia, denitrification, and N2O production in the ocean and their sensitivities to dissolved O2. Glob Biogeochem Cycles 26. https://doi.org/10.1029/2011GB004209
- Zumft WG. 1997. Cell biology and molecular basis of denitrification. Microbiol Mol Biol Rev 61:533–616. https://doi.org/10.1128/mmbr.61.4. 533-616.1997
- Sanford RA, Wagner DD, Wu Q, Chee-Sanford JC, Thomas SH, Cruz-García C, Rodríguez G, Massol-Deyá A, Krishnani KK, Ritalahti KM, Nissen S, Konstantinidis KT, Löffler FE. 2012. Unexpected nondenitrifier nitrous oxide reductase gene diversity and abundance in soils. Proc Natl Acad Sci USA 109:19709–19714. https://doi.org/10.1073/pnas.1211238109
- Bertagnolli AD, Konstantinidis KT, Stewart FJ. 2020. Non denitrifier nitrous oxide reductases dominate marine biomes. Environ Microbiol Rep 12:681–692. https://doi.org/10.1111/1758-2229.12879
- Lam P, Kuypers MMM. 2011. Microbial nitrogen cycling processes in oxygen minimum zones. Ann Rev Mar Sci 3:317–345. https://doi.org/10. 1146/annurev-marine-120709-142814
- Lüke C, Speth DR, Kox MAR, Villanueva L, Jetten MSM. 2016. Metagenomic analysis of nitrogen and methane cycling in the Arabian sea oxygen minimum zone. PeerJ 4:e1924. https://doi.org/10.7717/peerj. 1924
- Fuchsman CA, Devol AH, Saunders JK, McKay C, Rocap G. 2017. Niche partitioning of the N cycling microbial community of an offshore oxygen deficient zone. Front Microbiol 8:2384. https://doi.org/10.3389/fmicb. 2017.02384
- Rattanasriampaipong R, Zhang YG, Pearson A, Hedlund BP, Zhang S. 2022. Archaeal lipids trace ecology and evolution of marine ammoniaoxidizing archaea. Proc Natl Acad Sci USA 119:e2123193119. https://doi. org/10.1073/pnas.2123193119
- DeLong EF. 2020. Exploring marine planktonic archaea: then and now. Front Microbiol 11:616086. https://doi.org/10.3389/fmicb.2020.616086
- Zhang IH, Sun X, Jayakumar A, Fortin SG, Ward BB, Babbin AR. 2023. Partitioning of the denitrification pathway and other nitrite metabolisms within global oxygen deficient zones. ISME Commun 3:76. https://doi. org/10.1038/s43705-023-00284-y
- Glass JB, Kretz CB, Ganesh S, Ranjan P, Seston SL, Buck KN, Landing WM, Morton PL, Moffett JW, Giovannoni SJ, Vergin KL, Stewart FJ. 2015. Metaomic signatures of microbial metal and nitrogen cycling in marine oxygen minimum zones. Front Microbiol 6:998. https://doi.org/10.3389/ fmicb.2015.00998
- 47. Tsementzi D, Wu J, Deutsch S, Nath S, Rodriguez-R LM, Burns AS, Ranjan P, Sarode N, Malmstrom RR, Padilla CC, Stone BK, Bristow LA, Larsen M, Glass JB, Thamdrup B, Woyke T, Konstantinidis KT, Stewart FJ. 2016. SAR11 bacteria linked to ocean anoxia and nitrogen loss. Nature 536:179–183. https://doi.org/10.1038/nature19068
- Stewart FJ, Ulloa O, DeLong EF. 2012. Microbial metatranscriptomics in a permanent marine oxygen minimum zone. Environ Microbiol 14:23–40. https://doi.org/10.1111/j.1462-2920.2010.02400.x
- Ganesh S, Parris DJ, DeLong EF, Stewart FJ. 2014. Metagenomic analysis of size-fractionated picoplankton in a marine oxygen minimum zone. ISME J 8:187–211. https://doi.org/10.1038/ismej.2013.144
- Parks DH, Imelfort M, Skennerton CT, Hugenholtz P, Tyson GW. 2015. CheckM: assessing the quality of microbial genomes recovered from isolates, single cells, and metagenomes. Genome Res 25:1043–1055. https://doi.org/10.1101/gr.186072.114
- Chaumeil P-A, Mussig AJ, Hugenholtz P, Parks DH, Hancock J. 2019.
 GTDB-TK: a toolkit to classify genomes with the genome taxonomy database. Bioinformatics 36:1925–1927. https://doi.org/10.1093/bioinformatics/btz848

- Seemann T. 2014. Prokka: rapid prokaryotic genome annotation. Bioinformatics 30:2068–2069. https://doi.org/10.1093/bioinformatics/ btu153
- Pedruzzi I, Rivoire C, Auchincloss AH, Coudert E, Keller G, de Castro E, Baratin D, Cuche BA, Bougueleret L, Poux S, Redaschi N, Xenarios I, Bridge A. 2015. HAMAP in 2015: updates to the protein family classification and annotation system. Nucleic Acids Res 43:D1064– D1070. https://doi.org/10.1093/nar/gku1002
- Mistry J, Chuguransky S, Williams L, Qureshi M, Salazar GA, Sonnhammer ELL, Tosatto SCE, Paladin L, Raj S, Richardson LJ, Finn RD, Bateman A. 2021. Pfam: the protein families database in 2021. Nucleic Acids Res 49:D412–D419. https://doi.org/10.1093/nar/gkaa913
- Olm MR, Brown CT, Brooks B, Banfield JF. 2017. dRep: a tool for fast and accurate genomic comparisons that enables improved genome recovery from metagenomes through de-replication. ISME J 11:2864–2868. https://doi.org/10.1038/ismej.2017.126
- Delmont TO, Quince C, Shaiber A, Esen ÖC, Lee ST, Rappé MS, McLellan SL, Lücker S, Eren AM. 2018. Nitrogen-fixing populations of planctomycetes and proteobacteria are abundant in surface ocean metagenomes. Nat Microbiol 3:804–813. https://doi.org/10.1038/s41564-018-0176-9
- Lee MD. 2019. GToTree: a user-friendly workflow for phylogenomics.
 Bioinformatics 35:4162–4164. https://doi.org/10.1093/bioinformatics/btz188
- Nguyen L-T, Schmidt HA, von Haeseler A, Minh BQ. 2015. IQ-TREE: a fast and effective stochastic algorithm for estimating maximum-likelihood phylogenies. Mol Biol Evol 32:268–274. https://doi.org/10.1093/molbev/ msu300
- Hoang DT, Chernomor O, von Haeseler A, Minh BQ, Vinh LS. 2018. UFBoot2: improving the ultrafast bootstrap approximation. Mol Biol Evol 35:518–522. https://doi.org/10.1093/molbev/msx281
- Eren AM, Kiefl E, Shaiber A, Veseli I, Miller SE, Schechter MS, Fink I, Pan JN, Yousef M, Fogarty EC, et al. 2021. Community-led, integrated, reproducible multi-omics with anvi'o. Nat Microbiol 6:3–6. https://doi. org/10.1038/s41564-020-00834-3
- Kanehisa M, Goto S. 2000. KEGG: kyoto encyclopedia of genes and genomes. Nucleic Acids Res 28:27–30. https://doi.org/10.1093/nar/28.1. 27
- Tatusov RL, Fedorova ND, Jackson JD, Jacobs AR, Kiryutin B, Koonin EV, Krylov DM, Mazumder R, Mekhedov SL, Nikolskaya AN, Rao BS, Smirnov S, Sverdlov AV, Vasudevan S, Wolf YI, Yin JJ, Natale DA. 2003. The COG database: an updated version includes eukaryotes. BMC Bioinformatics 4:41. https://doi.org/10.1186/1471-2105-4-41
- Waterhouse AM, Procter JB, Martin DMA, Clamp M, Barton GJ. 2009.
 Jalview version 2: a multiple sequence alignment and analysis workbench. Bioinformatics 25:1189–1191. https://doi.org/10.1093/bioinformatics/btp033
- Hallgren J, Tsirigos KD, Pedersen MD, Almagro Armenteros JJ, Marcatili P, Nielsen H, Krogh A, Winther O. 2022. DeepTMHMM predicts alpha and beta transmembrane proteins using deep neural networks. bioRxiv. https://doi.org/10.1101/2022.04.08.487609
- 65. Edgar RC. 2010. Search and clustering orders of magnitude faster than BLAST. Bioinformatics 26:2460–2461. https://doi.org/10.1093/bioinformatics/btq461
- Katoh K, Standley DM. 2013. MAFFT multiple sequence alignment software version 7: improvements in performance and usability. Mol Biol Evol 30:772–780. https://doi.org/10.1093/molbev/mst010
- Capella-Gutiérrez S, Silla-Martínez JM, Gabaldón T. 2009. trimAl: a tool for automated alignment trimming in large-scale phylogenetic analyses. Bioinformatics 25:1972–1973. https://doi.org/10.1093/bioinformatics/ btp348
- Wilbert SA, Newman DK. 2022. The contrasting roles of nitric oxide drive microbial community organization as a function of oxygen presence. Curr Biol 32:5221–5234. https://doi.org/10.1016/j.cub.2022.10.008
- Zucko J, Dunlap WC, Shick JM, Cullum J, Cercelet F, Amin B, Hammen L, Lau T, Williams J, Hranueli D, Long PF. 2010. Global genome analysis of the shikimic acid pathway reveals greater gene loss in host-associated than in free-living bacteria. BMC Genomics 11:628. https://doi.org/10. 1186/1471-2164-11-628
- Tästensen J-B, Johnsen U, Reinhardt A, Ortjohann M, Schönheit P. 2020.
 D-galactose catabolism in archaea: operation of the DeLey–Doudoroff

- pathway in Haloferax volcanii. FEMS Microbiol Lett 367:fnaa029. https://doi.org/10.1093/femsle/fnaa029
- Hove-Jensen B, Andersen KR, Kilstrup M, Martinussen J, Switzer RL, Willemoës M. 2017. Phosphoribosyl diphosphate (PRPP): biosynthesis, enzymology, utilization, and metabolic significance. Microbiol Mol Biol Rev 81:00040-16. https://doi.org/10.1128/MMBR.00040-16
- Castelle CJ, Méheust R, Jaffe AL, Seitz K, Gong X, Baker BJ, Banfield JF.
 2021. Protein family content uncovers lineage relationships and bacterial pathway maintenance mechanisms in DPANN archaea. Front Microbiol 12:660052. https://doi.org/10.3389/fmicb.2021.660052
- Peters JW, Schut GJ, Boyd ES, Mulder DW, Shepard EM, Broderick JB, King PW, Adams MWW. 2015. [FeFe]- and [NiFe]-hydrogenase diversity, mechanism, and maturation. Biochim Biophys Acta BBA - Mol cell Res 1853:1350–1369.
- 74. Lappan R, Shelley G, Islam ZF, Leung PM, Lockwood S, Nauer PA, Jirapanjawat T, Ni G, Chen Y-J, Kessler AJ, Williams TJ, Cavicchioli R, Baltar F, Cook PLM, Morales SE, Greening C. 2023. Molecular hydrogen in seawater supports growth of diverse marine bacteria. Nat Microbiol 8:581–595. https://doi.org/10.1038/s41564-023-01322-0
- Pearson WR. 2013. An introduction to sequence similarity ("Homology") searching. Curr Protoc Bioinforma Ed Board Andreas Baxevanis Al 0 3 Chapter 3:3. https://doi.org/10.1002/0471250953.bi0301s42
- Zhang L, Wüst A, Prasser B, Müller C, Einsle O. 2019. Functional assembly of nitrous oxide reductase provides insights into copper site maturation. Proc Natl Acad Sci USA 116:12822–12827. https://doi.org/10.1073/pnas. 1903819116
- Kroneck PMH. 2018. Walking the seven lines: binuclear copper A in cytochrome C oxidase and nitrous oxide reductase. J Biol Inorg Chem 23:27–39. https://doi.org/10.1007/s00775-017-1510-z
- Farrar JA, Zumft WG, Thomson AJ. 1998. CuA and Cuz are variants of the electron transfer center in nitrous oxide reductase. Proc Natl Acad Sci USA 95:9891–9896. https://doi.org/10.1073/pnas.95.17.9891
- Zhang L, Bill E, Kroneck PMH, Einsle O. 2021. A [3Cu:25] cluster provides insight into the assembly and function of the CuZ site of nitrous oxide reductase. Chem Sci 12:3239–3244. https://doi.org/10.1039/d0sc05204c
- Babbin AR, Bianchi D, Jayakumar A, Ward BB. 2015. Rapid nitrous oxide cycling in the suboxic ocean. Science 348:1127–1129. https://doi.org/10. 1126/science.aaa8380
- Ji Q, Babbin AR, Jayakumar A, Oleynik S, Ward BB. 2015. Nitrous oxide production by nitrification and denitrification in the Eastern tropical South Pacific oxygen minimum zone. Geophys Res Lett 42:10. https:// doi.org/10.1002/2015GL066853
- Peng X, Fuchsman CA, Jayakumar A, Warner MJ, Devol AH, Ward BB. 2016. Revisiting nitrification in the Eastern tropical South Pacific: a focus on controls. J Geophys Res Oceans 121:1667–1684. https://doi.org/10. 1002/2015JC011455
- Naqvi SWA, Yoshinari T, Jayakumar DA, Altabet MA, Narvekar PV, Devol AH, Brandes JA, Codispoti LA. 1998. Budgetary and biogeochemical implications of N2O isotope signatures in the Arabian sea. Nature 394:462–464. https://doi.org/10.1038/28828
- Bourbonnais A, Letscher RT, Bange HW, Échevin V, Larkum J, Mohn J, Yoshida N, Altabet MA. 2017. N2O production and consumption from stable isotopic and concentration data in the Peruvian coastal upwelling system. Global Biogeochemical Cycles 31:678–698. https://doi.org/10. 1002/2016GB005567
- Kempes CP, van Bodegom PM, Wolpert D, Libby E, Amend J, Hoehler T. 2017. Drivers of bacterial maintenance and minimal energy requirements. Front Microbiol 8:31. https://doi.org/10.3389/fmicb.2017.00031
- Sakai HD, Nur N, Kato S, Yuki M, Shimizu M, Itoh T, Ohkuma M, Suwanto A, Kurosawa N. 2022. Insight into the symbiotic lifestyle of DPANN archaea revealed by cultivation and genome analyses. Proc Natl Acad Sci USA 119:e2115449119. https://doi.org/10.1073/pnas.2115449119
- Chronopoulou P-M, Shelley F, Pritchard WJ, Maanoja ST, Trimmer M. 2017. Origin and fate of methane in the Eastern tropical North Pacific oxygen minimum zone. ISME J 11:1386–1399. https://doi.org/10.1038/ ismej.2017.6
- Bird JT, Baker BJ, Probst AJ, Podar M, Lloyd KG. 2016. Culture independent genomic comparisons reveal environmental adaptations for Altiarchaeales. Front Microbiol 7:1221. https://doi.org/10.3389/fmicb. 2016.01221

- 89. Li L, Liu Z, Zhou Z, Zhang M, Meng D, Liu X, Huang Y, Li X, Jiang Z, Zhong S, Drewniak L, Yang Z, Li Q, Liu Y, Nan X, Jiang B, Jiang C, Yin H. 2021. Comparative genomics provides insights into the genetic diversity and evolution of the DPANN superphylum. mSystems 6:e0060221. https://doi.org/10.1128/mSystems.00602-21
- Probst AJ, Weinmaier T, Raymann K, Perras A, Emerson JB, Rattei T, Wanner G, Klingl A, Berg IA, Yoshinaga M, Viehweger B, Hinrichs K-U, Thomas BC, Meck S, Auerbach AK, Heise M, Schintlmeister A, Schmid M, Wagner M, Gribaldo S, Banfield JF, Moissl-Eichinger C. 2014. Biology of a widespread uncultivated archaeon that contributes to carbon fixation in the subsurface. Nat Commun 5:1. https://doi.org/10.1038/ncomms6497
- 91. Lipsewers YA, Hopmans EC, Sinninghe Damsté JS, Villanueva L. 2018. Potential recycling of thaumarchaeotal lipids by DPANN archaea in

- seasonally hypoxic surface marine sediments. Org Geochem 119:101–109. https://doi.org/10.1016/j.orggeochem.2017.12.007
- Gfrerer S, Winkler D, Novion Ducassou J, Couté Y, Rachel R, Gescher J. 2022. A micrarchaeon isolate is covered by a proteinaceous S-layer. Appl Environ Microbiol 88:e0155321. https://doi.org/10.1128/AEM.01553-21
- Brown K, Tegoni M, Prudêncio M, Pereira AS, Besson S, Moura JJ, Moura I, Cambillau C. 2000. A novel type of catalytic copper cluster in nitrous oxide reductase. Nat Struct Biol 7:191–195. https://doi.org/10.1038/ 73288
- Palumbo AV, Ferguson RL, Rublee PA. 1984. Size of suspended bacterial cells and association of heterotrophic activity with size fractions of particles in Estuarine and Coastal waters. Appl Environ Microbiol 48:157– 164. https://doi.org/10.1128/aem.48.1.157-164.1984